

## Time course of acute phase in mouse spinal cord injury monitored by ex vivo quantitative MRI

Manuel Gaviria,<sup>a,\*</sup> Jean-Marie Bonny,<sup>b</sup> Henri Haton,<sup>c</sup> Beatrix Jean,<sup>c</sup>  
Marisa Teigell,<sup>a</sup> Jean-Pierre Renou,<sup>b</sup> and Alain Privat<sup>c</sup>

<sup>a</sup>Neurêva Inc.-INM, CHU St Eloi, 80 rue Augustin Fliche, 34295 Montpellier, France

<sup>b</sup>STIM Unité QuaPA-INRA, Centre de Theix, 63122 Saint-Genès Champanelle, France

<sup>c</sup>INSERM U583-INM, CHU St Eloi, 80 rue Augustin Fliche, 34295 Montpellier, France

Received 30 August 2005; revised 23 December 2005; accepted 19 January 2006

Available online 20 March 2006

During the acute phase of spinal cord injury (SCI), major alterations of white and grey matter are a key issue, which determine the neurological outcome. The present study with ex vivo quantitative high-field magnetic resonance microimaging (MRI) was intended in order to identify sensitive parameters of tissue disruption in a well-controlled mouse model of ischemic SCI. MR imaging evidenced changes as early as the second hour after the lesion in the dorsal horns, which appear swollen. After 4 h, alterations of the white matter of dorsal and lateral funiculi were reflected by a progressive loss of white/grey matter contrast with further ventral extension by the 24th hour. Diffusion tensor imaging and multi-exponential  $T_2$  measurements permitted to quantify these physicochemical, time-related, alterations during the 24-h period. This characterization of spatial and temporal evolution of SCI will contribute to better define both the most appropriate targets for future therapies and more accurate therapeutic windows. Upcoming directions include the use of these parameters on in vivo animal models and their application to clinics. Indeed, magnetic resonance techniques appear now as a major non-invasive translation tool in CNS pathologies based on the development of more appropriate pre-clinical models.

© 2006 Elsevier Inc. All rights reserved.

### Introduction

Spinal cord injury (SCI) induces structural and functional modifications of neuronal networks yielding significant sensorimotor alterations. Thus, the interruption of long myelinated tracts and the disruption of local non-myelinated circuitry lead to specific neurological deficits. One of the major gaps in the development of an efficient therapeutic agent in the field of neuroprotection lies in the obviously poor adequacy of the pre-clinical approaches and their lack of predictability for the considered pathology (Blight,

2002). Actually, the therapeutic windows for neuroprotection have not been precisely pre-clinically established since the time dimension of the degenerative phenomenon is insufficiently known. Moreover, the correspondence with human pathophysiology is still inadequate.

Non-invasive techniques for analyzing the evolution of SCI are mandatory in order to accurately determine the time window of tissue alterations due to major neurotoxic events and thus, to elaborate more predictable animal models. Recent progresses of magnetic resonance imaging (MRI) bring the possibility of following in a non-invasive manner a pathophysiological process in spinal cord of rodents. Even if in vivo MRI has been already performed (Bonny et al., 2004; Bilgen et al., 2005; Kim et al., 2005), the choice of ex vivo MRI was governed by several advantages of this approach. Indeed, it is possible to extend the acquisition time in order to, on the one hand, increase the spatial resolution and thus define more accurately the extension of the injured areas, and on the other hand, to use quantitative techniques by the bias of multi-parametric reconstruction (Bonny, 2005). Finally, the definition of the time period between the induction of the lesion and fixing/observing the spinal cord is entirely free (in this case 2, 4, 8, 16, and 24 h after the injury; see below).

The sensitivity of ex vivo quantitative MRI has been exemplified for characterizing several pathological models in the rat spinal cord (Matsuzawa et al., 1995; Inglis et al., 1999; Nevo et al., 2001; Gulani et al., 2001; Nossin-Manor et al., 2002). In a mouse model of experimental allergic encephalomyelitis, reduced anisotropy in WM has been detected by diffusion tensor imaging (DTI) (Ahrens et al., 1998).

In the present study, mice were preferred to rats despite their smaller size since they give access to the extensive transgenic mice library opening the possibility of testing specific molecular hypotheses (Steward et al., 1999; Bonny et al., 2004).

To characterize our SCI model, the use of diffusion contrast is an obvious choice due to its sensitivity to acute ischemia (Moseley et al., 1990a,b). The decrease of apparent diffusion coefficient (ADC) is directly related to the degree of perfusion deficit (Fiehler

\* Corresponding author. Fax: +33 499 63 60 85.

E-mail address: gaviria@neureva.com (M. Gaviria).

Available online on ScienceDirect (www.sciencedirect.com).

et al., 2001). In our case, the diffusion characterization has been extended to the quantification of the apparent diffusion tensor (Basser et al., 1994). Compared to the estimation of ADC in a fixed direction, diffusion tensor gives access to the three-dimensional diffusive transport of water. It provides multiple parameters (diffusivities, anisotropy and principal direction of diffusion) which are influenced by microstructural components of the tissue and in particular have been proven sensitive for the characterization of stroke lesions (Sotak, 2002).

Besides diffusion imaging which assesses the severity of the earliest ischemic events, quantitative  $T_2$  imaging is a useful complementary technique since the elevated  $T_2$  values give information about the extent and the degree of vasogenic edema during ischemia (Helpert et al., 1993; Loubinoux et al., 1997). Moreover, most of the biological tissues exhibit multiple  $T_2$  components in the range measurable by imaging. Previous relaxation studies of peripheral nerves (Jolesz et al., 1987) and myelinated WM (MacKay et al., 1994) suggest that the shortest measured  $T_2$  represents water associated to the myelin membranes. Moreover, the size of this short- $T_2$  component is well correlated with the myelin content in fixed samples of normal and injured rat nerves (Webb et al., 2003). Because of the potential of this approach for detecting myelin loss after injury, the  $T_2$  relaxation curves have been sampled densely in our experimental protocol to detect possible multi-exponential behavior in white matter.

In the present study, we followed the evolution of quantitative parameters obtained from DTI and multi-exponential  $T_2$  imaging ( $MET_2$ ) during the time course of an ischemic experimental lesion in the mouse spinal cords. The time frame was that of acute phase (<24 h after lesion induction) which constitutes a critical period that strongly determines posttraumatic neurological impairment and the pharmacological windows for neuroprotection (Gimenez y Ribotta and Privat, 1998).

## Materials and methods

### Animal preparation

Twenty-eight female C57BL/6 mice (Charles River Laboratories, L'Arbresle, France), aged 16–18 weeks ( $20 \pm 3$  g) were used in this study. This strain was chosen on the basis of its wide utilization in CNS pathological models and its high degree of genetic differentiation (Steward et al., 1999). The study was performed according to European legislative, administrative and statutory measures concerning the protection of animals used for experimental or other scientific purposes (86/609/EEC). All mice, except for controls, were submitted to an experimental ischemic spinal cord lesion (Gaviria et al., 2002). Animals were divided into six groups depending on the time of sacrifice: controls ( $n = 4$ ), 2 h ( $n = 4$ ), 4 h ( $n = 4$ ), 8 h ( $n = 6$ ), 16 h ( $n = 5$ ), and 24 h ( $n = 5$ ) postinjury.

Animals were anesthetized through a mask by spontaneous inhalation of 2% isoflurane in a current volume of 200 ml of air/min using a Univentor 400 anesthesia unit (Univentor Ltd., Malta). After obtaining a deep level of anesthesia judged by a loss of response to nociceptive stimulation of the footpads and tail, mice were placed in a prone position on a warmed surgical surface to preserve body temperature throughout the procedure, i.e.,  $\pm 1.5^\circ\text{C}$  of the initial temperature, with a heating pad (Homeothermic Blanket Control Unit, Harvard Apparatus, Edenbridge, USA). A midline longitudinal incision was made over the T5 to T13 level.

The skin was retracted, and the fat pad was carefully reflected rostrally taking into account its important vascular supply present at the T6–T7 level. The vertebral muscles were dissected bilaterally exposing the dorsal laminae and spinous processes of T7–T10 vertebrae.

Immediately after the end of the surgical procedure on the back, Rose Bengal (Aldrich Chemical Co., Milwaukee, USA) was intravenously injected (0.0133 ml/10 g, 30 mg/ml in 0.9% saline) on the tail vein by means of a polyethylene 1 French-catheter over a 3-min period. The skin of the tail was then sutured, and the animal was transferred to the irradiation apparatus (ILC Technology, Sunnyvale, USA). Ten minutes after the injection of Rose Bengal, animals were irradiated for 8 min (Gaviria et al., 2002). For this purpose, the irradiation beam of a xenon lamp, conveyed by fiberoptics, was focused over the T8 vertebrae. A 560-nm wavelength-light irradiation was performed over the translucent dorsal surface of the vertebral laminae, inducing excitation of the injected dye, i.e., Rose Bengal, in the spinal cord microvasculature. A dual fan system was used to maintain body temperature at a standard level at the irradiation site to avoid thermal injury. The resultant photochemical reaction is known to provoke luminal platelet aggregation, endothelial membrane damage, and blood–brain barrier disruption. Actually, Rose Bengal is the most efficient known generator of singlet oxygen in terms of reacting with structural proteins and lipids in order to initiate direct peroxidation reactions within endothelial membranes resulting in vascular stasis, parenchymal thrombosis and ischemia (Watson et al., 1986). After irradiation, the back muscles were sutured with 4-0 vicryl (Ethicon SAS, Issy les Moulineaux, France) and the skin closed with tissue adhesive (*N*-butyl-2-cyanoacrylate, B/Braun Germany). After total recovery from anesthesia (~10 min), the animals were returned to their individual cages.

At the time of sacrifice, animals were re-anesthetized and perfused through the heart with a solution of paraformaldehyde according to our protocol for ex vivo preparation (Bonny et al., 2004). The vertebral column was left overnight in situ at  $4^\circ\text{C}$ , then a block of 5 vertebrae, i.e., 2 vertebral bodies above and below the T8 vertebral body (epicenter of the photothrombotic lesion), was removed and postfixed for at least 24 h at  $4^\circ\text{C}$  in the same fixative.

After ex vivo MRI examination, the spinal cord was prepared for histological analysis (see Gaviria et al., 2002). Five sets of cryostat transverse 12- $\mu\text{m}$ -thick sections, corresponding to each vertebral level (mid vertebral body landmark) and covering each thoracic metamer, i.e., T6 to T10, were obtained for histological staining of white and grey matter (luxol fast blue/neutral red). The advantage of this method over other standard staining techniques is to label both the intact myelin and cells cytoplasm permitting to characterize myelin and neuronal changes. The sections were examined under light microscopy, and photomicrographs were matched with corresponding MRI images. Nevertheless, in spite of a systematic location of spinal cord marks, gross morphological characteristics of the 12- $\mu\text{m}$ -thick sections differ slightly from MR images presumably because of the partial volume effect due to the 1 mm slice thickness of the latter (covering almost the whole spinal cord metamer).

### MRI parameters

During MRI analysis, each cord was transferred from the fixative to a phosphate buffering saline solution (PBS) and placed in a 5-mm diameter microimaging probe. Experiments were

performed at 37°C on an Avance DRX400 microimaging system (Bruker, GmbH, Ettlingen, Germany) with a wide-bore (89 mm) vertical 9.4 T magnet and an actively shielded gradient coil allowing a maximum gradient strength of 1000 mT/m. For both DTI and  $MET_2$ , images of five slices cut perpendicularly to the spinal cord were collected; each 1-mm-thick slice covered a single thoracic metamer. The voxel size is equal to  $0.04 \times 0.04 \text{ mm}^3$  (field of view of  $5 \times 5 \text{ mm}^2$ , image matrix of  $128 \times 64$  zero filled to  $128 \times 128$ ).

For DTI, the imaging protocol used a diffusion-weighted spin echo sequence with the following parameters: TR = 5000 ms, TE = 26.9 ms, NA = 8, readout bandwidth of 39 Hz/pixel,  $\Delta = 6.0$ -ms duration,  $\delta = 2.5$  ms and  $b$  value of  $900 \text{ s.mm}^{-2}$ . Diffusion weighted images were acquired along 6 non-collinear directions, along with a single image acquired without diffusion sensitizing gradients (Basser and Pierpaoli, 1998).

The sequence for  $T_2$ -mapping consisted of collecting 16 images at increasing TE with a single spin echo for each. By collecting a single spin echo per scan, the protocol prevents the repetition of refocusing errors that induces both the underestimation of  $T_2$  due to the accumulation of fractional signal loss and the generation of undesired additional echoes. The  $MET_2$  protocol consisted of 16 spin echo images with equidistant TE ranging from 12.5 ms to 87.6 ms (inter-echo delay of 5 ms). Other acquisition parameters were TR = 5000 ms, NA = 4 along with a readout bandwidth of 195 Hz/pixel.

The whole protocol led to a total acquisition time of 12 h.

### Postprocessing

The diffusion tensor was estimated using a multivariate linear regression routine. After tensor diagonalization which leads to the ordered eigenvalues ( $\lambda_1 > \lambda_2 > \lambda_3$ ) and assuming an axisymmetric diffusion model, axial diffusivity  $\lambda_{//}$  ( $=\lambda_1$ ) and radial diffusivity  $\lambda_{\perp}$  ( $=(\lambda_2 + \lambda_3)/2$ ) were computed.

Discrete multi-exponential analysis of  $T_2$  relaxation decay curves consisted of a multi-spectral nonlinear edge-preserving filter followed by a non-linear least squares procedure (Bonny et al., 2003). Because of the limitation in the number and the range of TE, this analysis is able to resolve at best two  $T_2$  components. Each component is characterized by a relaxation time and an amplitude (i.e., in the bi-exponential case the parameters measured are long- $T_2$ , short- $T_2$  and relative amplitude of the short- $T_2$ ).

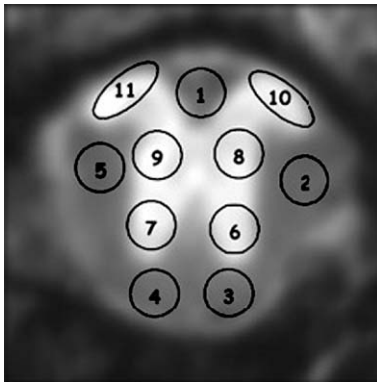


Fig. 1. ROI in spinal axial plane; WM (1) dorsal funiculus, (2/5) lateral funiculi, (3/4) ventral funiculi, GM (6/7) ventral horns, (8/9) zona intermedia lateralis, (10/11) dorsal horns substantia gelatinosa.

The values of the different parameters were measured by positioning 11 regions of interest (ROI) in the parametric maps of the spinal cord (see Fig. 1).

For statistical analysis, the values are presented as means and both standard deviation (SD) and standard error of the mean (SEM). An ANOVA test was applied to determine significant time-related differences in MRI parameters followed by a Newman–Keuls multiple comparison post hoc tests. A  $P$  level of 0.05 was considered statistically significant. GraphPad Prism software (GraphPad Software Incorporated, San Diego, CA, USA) was used for statistical analysis.

### Results

Control samples were pooled for WM values (5 ROI: dorsal, lateral, and ventral funiculi) and GM values (6 ROI: dorsal horns, zona intermedialateralis and ventral horns). The axial and radial diffusivities were respectively equal to  $1.37 \cdot 10^{-3}$  (SD = 0.12)  $\text{mm}^2/\text{s}$  and  $0.26 \cdot 10^{-3}$  (SD = 0.11)  $\text{mm}^2/\text{s}$  in WM and  $0.72 \cdot 10^{-3}$  (SD = 0.12)  $\text{mm}^2/\text{s}$  and  $0.42 \cdot 10^{-3}$  (SD = 0.04)  $\text{mm}^2/\text{s}$  in GM. These results point to a significant anisotropy for both tissues in accordance with previous ex vivo studies in mouse (Ahrens et al., 1998) and rat (Inglis et al., 1997; Inglis et al., 2001; Madi et al., 2004) spinal cord. Such diffusivities led to values of fractional anisotropy (Basser and Pierpaoli, 1996) significantly higher in WM than in GM, respectively 0.80 (SD = 0.08) and 0.36 (SD = 0.11).

Diffusion MRI changes were noticed at a very early stage after SCI within WM with a dorso-ventral cord gradient in accordance to injury mechanisms. As soon as the second hour after injury, parallel diffusion rapidly decreased and was significantly altered (30% decrease,  $P < 0.01$ ) within the dorsal funiculus, whereas in the lateral funiculi, significant changes were noticed between 4 and 8 h after SCI (50% decrease,  $P < 0.01$ ) (see Fig. 2). Twenty-four hours after injury, loss exceeded 70% in dorsal funiculus ( $P < 0.01$ ) and 60% in lateral funiculi ( $P < 0.01$ ). Whatever the delay after injury, the variations in ventral funiculi were non-significant. Interestingly indeed, earliest WM changes detected by parallel diffusion preceded those depicted by both MR images and histology (see above).

Conversely, no significant alterations were noticed for  $\lambda_{\perp}$  after SCI near the irradiation region (see Fig. 3). A significant increase of the radial diffusivity was only noticed at a much later time point (i.e., 24 h after SCI) in the ventral funiculi (50% increase, significantly different compared to 4-h and to 8-h values;  $P < 0.05$ ).

One of the novel aspects of this study is the association of a multi-exponential analysis of the  $T_2$  relaxation curves with the analysis of the diffusion tensor. In control tissues, the behavior of the relaxation curves is bi-exponential in the WM and, most often, mono-exponential in the GM (see Table 1).

During the development of spinal cord injury, two types of  $T_2$  behavior were noticed during the first 24 h: a trend for a concomitant decrease of the three parameters in WM (i.e., long- $T_2$ , short- $T_2$  and relative amplitude of the short- $T_2$ ), while the changes in GM were reflected by an increase in the number of ROI showing mono-exponential  $T_2$  behavior. Concerning the WM changes, the main trend was a dorso-ventral cord gradient. Within the dorsal funiculus, the decrease of short- $T_2$  amplitude was significant since the 4th hour after the initial injury, while it was significant since the 8th hour within the lateral funiculi. No

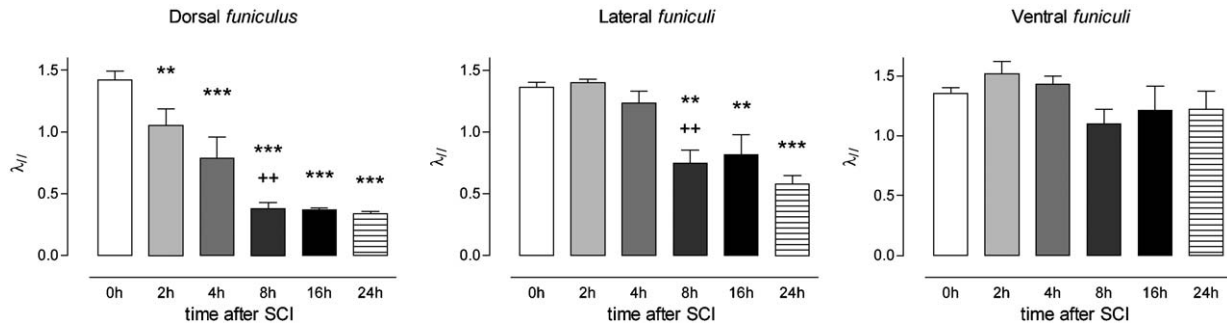


Fig. 2. Parallel diffusion measured within the different white matter ROI; (\*) corresponds to statistical differences between the group 0 h and the other groups and (+) to the difference between 4 h and 8 h; (\*\* or ++)  $P < 0.01$ , (\*\*\*)  $P < 0.001$ .

significant decrease was noticed within ventral funiculi despite the trend observed in Fig. 4. 24 h after injury, short- $T_2$  was absent in dorsal funiculus, the decrease exceeding 60% in lateral funiculi ( $P < 0.01$ ). Thus, a characterized critical time interval was noticed between 4 and 8 h within dorsal and lateral funiculi. For GM, the percentage of mono-exponential measurements progressively increased from 60% in the pooled ROI (dorsal horns, *zona intermediolateralis*, and ventral horns) of controls to 95% 24 h after SCI.

## Discussion

Several morphological changes observed after photochemical SCI (Prado et al., 1987; Bunge et al., 1994; Olby and Blakemore, 1996; Gaviria et al., 2002) have also been described after contusion or compression of the spinal cord (Gledhill et al., 1973; Bresnahan, 1978; Griffiths and McCulloch, 1983; Holtz et al., 1990; Blight, 1991). These histopathological similarities are mainly due to the fact that the chief mechanism of the secondary injury is posttraumatic ischemia and infarction of the spinal cord (Tator and Fehlings, 1991), involving common mechanisms of degeneration (for review of the secondary injury, see Choi, 1992). The vascular phenomenon first occurs in central GM and then spreads into WM tracts because of the greater concentration of blood vessels in GM compared to WM.

A pathophysiological condition like ischemia causes a massive increase in the extracellular glutamate concentration and the overstimulation of glutamate receptors triggers cellular processes leading to acute neurodegenerative conditions (for review, see Gimenez y Ribotta et al., 2002). Thus, NMDA receptors appear primarily responsible for rapidly triggered glutamate-induced cell

death mediated by a rapid influx of  $\text{Ca}^{2+}$  (Siesjo and Wieloch, 1985), and AMPA/kainate receptors for slowly triggered excitotoxicity in which the rate of  $\text{Ca}^{2+}$  influx is slower.

Interestingly, in the early acute phase, in spite of a normal appearance of axons and glia under light microscopy, electron microscopy reveals initial organelles changes, such as swollen mitochondria (Olby and Blakemore, 1996). During the first hours, histological alterations become apparent. Thus, platelet aggregation, degranulation, expansion of the extracellular space in WM and GM, intracellular GM vacuoles within the neuropil, initial GM necrosis, and perivascular glial swelling take place within the dorsal cord at the epicenter of the lesion. These changes are followed by further expansion of the extracellular space in WM/GM and accompanied by axonal swelling and necrosis, thinning of myelin sheets, extension of the area of GM necrosis, and edema. By twenty-four hours after the primary insult, the lesion is fully extended, and demyelination begins at the interface of necrotic and spared tissue (ventral-most WM). Other acute changes (24 to 48 h) such as axonal aggregates of organelles (mitochondria, vesicles, and neurofilaments) in varying states of deterioration and abundant myelin debris have also been described (Tator and Fehlings, 1991; Bunge et al., 1994; Olby and Blakemore, 1996).

In the present study, upon comparison of histological sections and MR images, it appeared that despite a lower spatial resolution, MR images matched very precisely the anatomical information given by luxol fast blue staining. Fig. 5 shows the development of SCI in high-resolution  $T_2$ -weighted images and in their histological correspondence. Swelling of dorsal horns was apparent as early as 2 to 4 h after the lesion, whereas the white matter appeared still intact, both with MR and histology. The spatial location of the initial GM changes can be due both to (i) the dorsal location of the primary injury and (ii) the distribution of NMDA receptors within

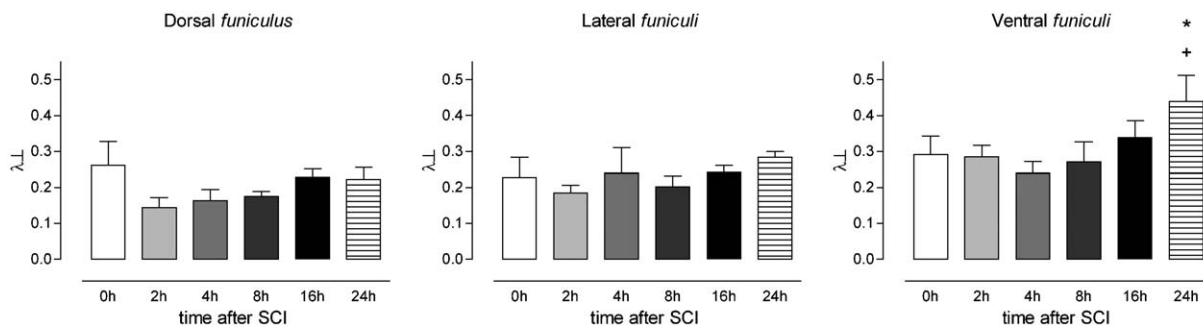


Fig. 3. Perpendicular diffusion measured within the different white matter ROI; (\*) corresponds to statistical differences between 4 h and 24 h and (+) to the difference between 8 h and 24 h; (\* or +)  $P < 0.05$ .

Table 1  
Control MET<sub>2</sub> values corresponding to non-injured spinal cords

	WM			GM (all)			GM (mono)			GM (bi)		
	Mean	SD	<i>n</i>	Mean	SD	<i>n</i>	Mean	SD	<i>n</i>	Mean	SD	<i>n</i>
<i>Data pooled (all ROI)</i>												
Long-T <sub>2</sub>	148.58	80.34	20	–	–	–	79.79	6.82	15	99.24	21.02	8
Short-T <sub>2</sub>	42.21	5.03	20	–	–	–	–	–	15	53.44	20.03	8
Amplitude percent	64.13	10.43	20	–	–	–	–	–	15	55.78	31.53	8
<i>Data pooled in the spinal cord region</i>												
Dorsal cord												
Long-T <sub>2</sub>	204.05	160.04	4	–	–	–	84.06	7.00	6	119.37	29.09	2
Short-T <sub>2</sub>	38.01	3.50	4	–	–	–	–	–	6	63.68	18.14	2
Amplitude percent	70.32	6.68	4	–	–	–	–	–	6	74.84	13.76	2
Lateral cord												
Long-T <sub>2</sub>	143.30	52.88	8	–	–	–	78.14	6.50	4	97.49	16.97	4
Short-T <sub>2</sub>	43.61	4.60	8	–	–	–	–	–	4	57.28	21.30	4
Amplitude percent	62.74	10.84	8	–	–	–	–	–	4	51.62	33.48	4
Ventral cord												
Long-T <sub>2</sub>	126.11	37.10	8	–	–	–	75.98	4.67	5	82.60	2.21	2
Short-T <sub>2</sub>	42.92	5.42	8	–	–	–	–	–	5	35.52	14.37	2
Amplitude percent	62.42	11.46	8	–	–	–	–	–	5	45.04	48.79	2

In the GM, the total number of values is 24, but there is a meaningless long-T<sub>2</sub> value within the ventral region which explains the size of the sample (*n* = 7 instead of 8) and the size of the complete data pool (*n* = 23 instead of 24).

neuronal populations of the GM. Actually, NMDA receptors are mainly present in dorsal horns and lamina IX, whereas in most other laminae (V–VIII), they are slightly labeled or unlabeled on binding experiments (Petralia et al., 1994; Hirbec et al., 2000). After 4 h, pallor of myelin noticed with luxol fast blue was paralleled by progressive MRI loss of contrast in dorsal and lateral funiculi, whereas grey matter edema progressed towards ventral horns. Gradual destruction of both white and grey matter, as seen in histological sections, was paralleled by loss of GM/WM contrast in MR images. On this basis, quantitative data obtained by DTI and MET<sub>2</sub> are likely to reflect physicochemical alterations of the nervous tissue induced by SCI which are complementary to classical anatomical examination.

In the whole central nervous system, diffusion anisotropy has been mainly reported in WM (Moseley et al., 1990a,b; Fenyves and Narayana, 1999). It corresponds to a more efficient diffusion of water parallel to the axonal direction axis than perpendicular to it. This property is the basis of non-invasive tractography of myelinated fibers in the central nervous system (Conturo et al., 1999) and is related to the ordered arrangement of these fibres. The

microstructural determinants of anisotropy have been reviewed by Beaulieu (2002).

The early decrease of parallel diffusivity in the WM indirectly indicates tissue structure alteration. It is associated with the cytotoxic edema, which appears during hyper-acute ischemic strokes. Both dorso-ventral and temporal gradients reflect the pathophysiological course of the ischemic phenomenon, which tends to broaden ventrally as highlighted by the Fig. 5. Our results suggest that the reduction of water translational motion in ischemic WM is mainly due to the reduction of the diffusivity parallel to the myelinated axons, in accordance with previous observations in human ischemic brains (Sorensen et al., 1999) and piglets (Thornton et al., 1997). Thus, the decrease of anisotropy in WM during the hyper-acute period can be mainly attributed to the decrease of  $\lambda_{//}$ , whereas  $\lambda_{\perp}$  remains stable.

More surprising is the increase of  $\lambda_{\perp}$  at +24 h, which is only significant in the ventral region, the most distant from the focus of the lesion. It corresponds to a pathologic state since  $\lambda_{\perp}$  is increased in comparison with its control value. This phenomenon would correspond to a demyelination process partially de-

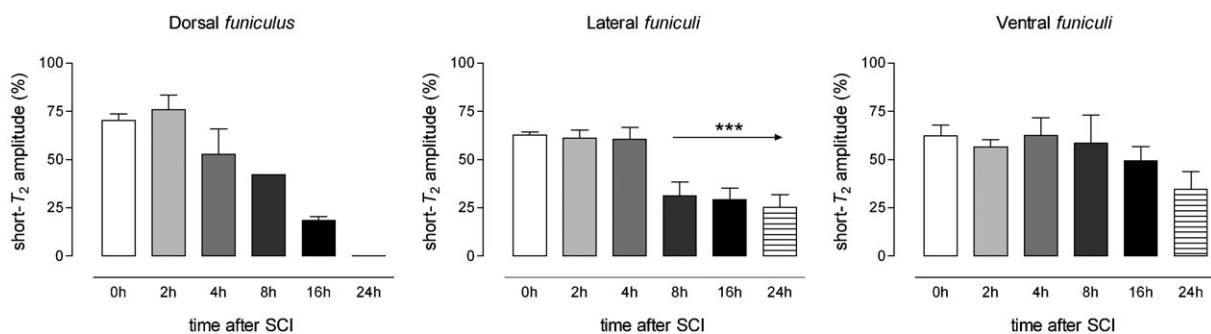


Fig. 4. Short-T<sub>2</sub> component of MET<sub>2</sub> measured within the different white matter ROI; (\*) corresponds to statistical differences between the groups 0 h, 2 h, 4 h, and the groups 8 h, 16 h and 24 h; (\*\*\*) *P* < 0.001. A statistical value could not be computed within the dorsal funiculus, as the progression of the lesion was followed by an increase in the number of ROI showing a mono-exponential T<sub>2</sub> behavior: *n*<sub>ROI</sub> = 1 8 h after SCI and *n*<sub>ROI</sub> = 0 24 h after SCI.

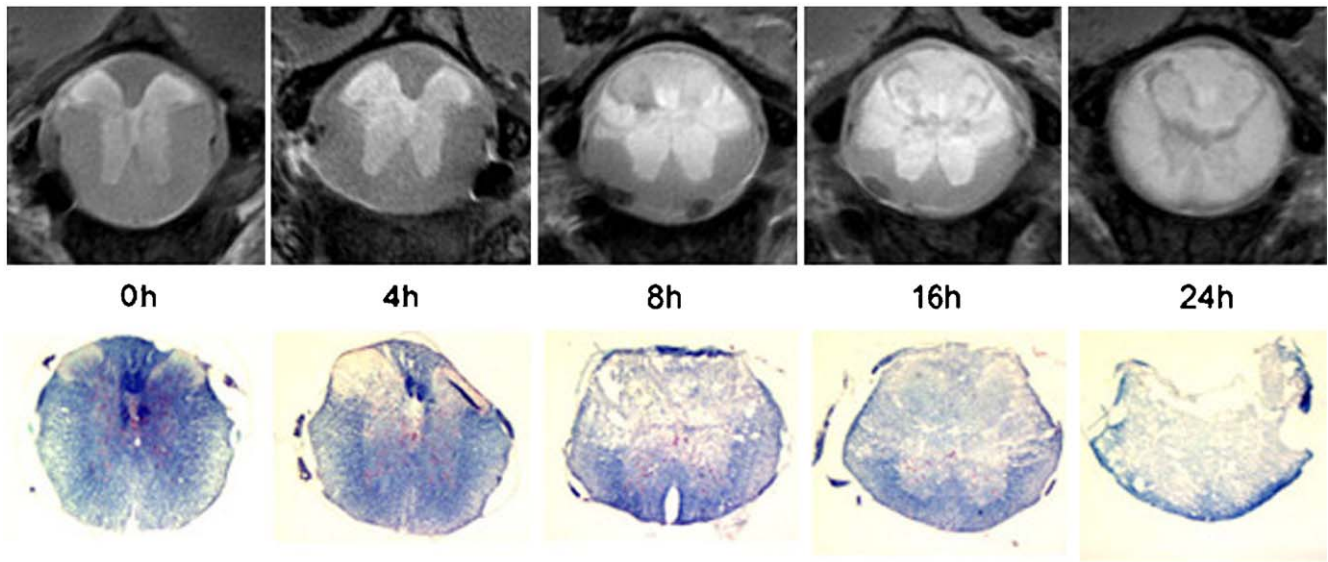


Fig. 5. High-resolution (acquisition matrix  $128 \times 128$ , zero filled to  $256 \times 256$  to obtain a voxel volume of  $60 \times 60 \times 200 \mu\text{m}^3$ )  $T_2$ -weighted (TR/TE = 5000/47 ms) and corresponding histological images for each measured time after SCI.

correlated from the cytotoxic edema, which is known to induce a specific increase of radial diffusivity (Song et al., 2005). The demyelination process takes place as a secondary degenerative component (Choi, 1992) at the interface between necrotic and spared tissue from the end of the first day after SCI (Griffiths and McCulloch, 1983). Actually, demyelination and remyelination phenomena have been described up to 450 days following contusive spinal cord injury in adult rats with an overall number of demyelinated axons peaking at 1 day postinjury (Totoiu and Keirstead, 2005). Thus, demyelination can be considered as a major target for therapeutic intervention after spinal trauma.

In GM, despite the typical swelling of the dorsal horns then of the whole grey matter due to the cytotoxic edema, no significant variation of diffusivities was observed. Even if a trend towards decrease was observed, especially dorsally, the inter-individual variations prevent the detection of a statistically significant decrease. Sotak (2002) pointed out several inconsistencies concerning the differential ADC response of WM and GM to ischemic injury. Our results clearly establish that the decrease of diffusivities is greater in WM than GM during the acute period.

Concerning  $T_2$  parameters, the bi-exponential behavior observed in the WM can be compared with the multi-exponential character often observed at lower fields in vivo (Whittall et al., 1997; Does and Gore, 2002) and ex vivo (Peled et al., 1999; Webb et al., 2003). In our experimental conditions, a smaller number of points (16 images with increasing TE), a relatively high minimum TE, as well as the probable reduction of the  $T_2$  values due to the increase of the field, certainly impede the detection of the short fraction associated to the water trapped by the myelin membranes themselves. The fractions observed in the present study may correspond to the intermediate fractions, which result from the slow exchange between the intra- and extra-axonal compartments. The hypothesis is that the exchange velocity between these two compartments is limited by the presence of myelin, which is particularly abundant around the axons in the spinal cord WM. This could explain what we observed in the control tissues, i.e., the bi-exponential behavior in the WM and the more frequently mono-exponential behavior in the GM. Thus, these parameters are also

sensitive indicators of the development of the ischemic lesion. The alteration of the amplitude of the short- $T_2$  component in WM may be explained by a demyelination.

Early alterations detected by quantitative MRI after SCI preceded those seen by histological techniques. This sensitiveness points to the broad coverage of MRI techniques, which allow detecting molecular changes within the neural tissue, whereas major and permanent structural alterations not yet took place in this time frame. The possibility to detect precocious molecular changes in vivo and to correlate them with neurochemical posttraumatic events, with a same animal being used as its own control, will represent a major breakthrough for the design of novel neuro-protective therapeutic strategies. Magnetic Resonance Spectroscopy has to be considered as a technique likely to enhance the characterization of SCI within the same regions of interest utilized for MRI. By considering the specific anatomy of mouse spinal cord, a maximum volume of  $0.4 \times 0.4 \times 1 \text{ mm}$  ( $0.16 \mu\text{l}$ ) would be reached within each ROI individually. Such small volume is clearly challenging in our experimental conditions since the volume currently obtained by localized spectroscopy is in the order of several microliters ( $\sim 16.5 \mu\text{l}$ ) (Silver et al., 2001). Therefore, simultaneous methodological breakthrough (i.e., ultra-high magnetic fields, implantable microcoils, powerful gradients) have to be fulfilled to obtain volumes of interest compatible for both MRI and MRS.

## Conclusion

Ischemia represents one of the main components of traumatic SCI. General and specific vascular alterations largely play a key role in the secondary injury process.

The present ex vivo MRI approach has permitted to identify and validate several quantitative parameters, which are sensitive enough to detect very early physicochemical changes after a well-calibrated ischemic spinal cord injury in mice. These accurate markers, i.e., the axial diffusivity measured at low  $b$  value and the fractions of the bi-exponential  $T_2$  components, constitute a unique tool for a

translational approach. Significant markers being identified, extension of MR investigation to in vivo conditions is achievable because of its biological relevance and its feasibility in spinal cord of various experimental animals such as rats (Ford et al., 1994, Pirko et al., 2005) and mice (Bonny et al., 2004, Bilgen et al., 2005). Even if diffusion MRI has already been achieved, the possibility to perform in vivo MET<sub>2</sub> imaging with both sufficient accuracy and acceptable acquisition times remains to be demonstrated.

The development of such a multidisciplinary methodology combining MR, morphologic and functional assessments will allow to define efficient therapeutic strategies and fine tuning windows for intervention in pre-clinical models before being applied in clinics.

### Acknowledgments

This work was supported by grants from the Institut National de la Santé et de la Recherche Médicale (INSERM—The National Institute of Health and Medical Research), the French Institute for Spinal Cord Research (IRME), Association Verticale, Fondation de l'Avenir (The Foundation for the Future), Fondation pour la Recherche Médicale (Foundation for Medical Research), and the DGA (the French equivalent of the DOD), and these assistance and help are gratefully acknowledged.

### References

- Ahrens, E.T., Laidlaw, D.H., Readhead, C., Brosnan, C.F., Fraser, S.E., Jacobs, R.E., 1998. MR microscopy of transgenic mice that spontaneously acquire experimental allergic encephalomyelitis. *Magn. Reson. Med.* 40, 119–132.
- Basser, P.J., Pierpaoli, C., 1996. Microstructural and physiological features of tissues elucidated by quantitative-diffusion-tensor MRI. *J. Magn. Reson.* B 111, 209–219.
- Basser, P.J., Pierpaoli, C., 1998. A simplified method to measure the diffusion tensor from seven MR images. *Magn. Reson. Med.* 39, 928–934.
- Basser, P.J., Mattiello, J., LeBihan, D., 1994. MR diffusion tensor spectroscopy and imaging. *Biophys. J.* 66, 259–267.
- Beaulieu, C., 2002. The basis of anisotropic water diffusion in the nervous system—A technical review. *NMR Biomed.* 15, 435–455.
- Bilgen, M., Al-Hafez, B., Festoff, B.W., 2005. Magnetic resonance imaging of mouse spinal cord. *Magn. Reson. Med.* 54, 1226–1231.
- Blight, A.R., 1991. Morphometric analysis of blood vessels in chronic experimental spinal cord injury: hypervascularity and recovery of function. *J. Neurol. Sci.* 106, 158–174.
- Blight, A.R., 2002. Miracles and molecules—progress in spinal cord repair. *Nat. Neurosci.* 5, 1051–1054 (Suppl.)
- Bonny, J.M., 2005. Methods and applications of quantitative MRI. *Annual Reports on NMR Spectroscopy*.
- Bonny, J.M., Boespflug-Tanguy, O., Zanca, M., Renou, J.P., 2003. Multi-exponential analysis of magnitude MR images using a quantitative multispectral edge-preserving filter. *J. Magn. Reson.* 161, 25–34.
- Bonny, J.M., Gaviria, M., Donnat, J.P., Jean, B., Privat, A., Renou, J.P., 2004. Nuclear magnetic resonance microimaging of mouse spinal cord in vivo. *Neurobiol. Dis.* 15, 474–482.
- Bresnahan, J.C., 1978. An electron-microscopic analysis of axonal alterations following blunt contusion of the spinal cord of the rhesus monkey (*Macaca mulatta*). *J. Neurol. Sci.* 37, 59–82.
- Bunge, M.B., Holets, V.R., Bates, M.L., Clarke, T.S., Watson, B.D., 1994. Characterization of photochemically induced spinal cord injury in the rat by light and electron microscopy. *Exp. Neurol.* 127, 76–93.
- Choi, D.W., 1992. Excitotoxic cell death. *J. Neurobiol.* 23, 1261–1276.
- Conturo, T.E., Lori, N.F., Cull, T.S., et al., 1999. Tracking neuronal fiber pathways in the living human brain. *Proc. Natl. Acad. Sci. U. S. A.* 96, 10422–10427.
- Does, M.D., Gore, J.C., 2002. Compartmental study of T(1) and T(2) in rat brain and trigeminal nerve in vivo. *Magn. Reson. Med.* 47, 274–283.
- Fenyves, D.A., Narayana, P.A., 1999. In vivo diffusion characteristics of rat spinal cord. *Magn. Reson. Imaging* 17, 717–722.
- Fiehler, J., Knab, R., Reichenbach, J.R., Fitzek, C., Weiller, C., Rother, J., 2001. Apparent diffusion coefficient decreases and magnetic resonance imaging perfusion parameters are associated in ischemic tissue of acute stroke patients. *J. Cereb. Blood Flow Metab.* 21, 577–584.
- Ford, J.C., Hackney, D.B., Joseph, P.M., et al., 1994. A method for in vivo high resolution MRI of rat spinal cord injury. *Magn. Reson. Med.* 31, 218–223.
- Gaviria, M., Haton, H., Sandillon, F., Privat, A., 2002. A mouse model of acute ischemic spinal cord injury. *J. Neurotrauma* 19, 205–221.
- Gimenez y Ribotta, M., Privat, A., 1998. Biological interventions for spinal cord injury. *Curr. Opin. Neurol.* 11, 647–654.
- Gimenez y Ribotta, M., Gaviria, M., Menet, V., Privat, A., 2002. Strategies for regeneration and repair in spinal cord traumatic injury. *Prog. Brain Res.* 137, 191–212.
- Gledhill, R.F., Harrison, B.M., McDonald, W.I., 1973. Demyelination and remyelination after acute spinal cord compression. *Exp. Neurol.* 38, 472–487.
- Griffiths, I.R., McCulloch, M.C., 1983. Nerve fibres in spinal cord impact injuries: Part 1. Changes in the myelin sheath during the initial 5 weeks. *J. Neurol. Sci.* 58, 335–349.
- Gulani, V., Webb, A.G., Duncan, I.D., Lauterbur, P.C., 2001. Apparent diffusion tensor measurements in myelin-deficient rat spinal cords. *Magn. Reson. Med.* 45, 191–195.
- Helpern, J.A., Dereski, M.O., Knight, R.A., Ordidge, R.J., Chopp, M., Qing, Z.X., 1993. Histopathological correlations of nuclear magnetic resonance imaging parameters in experimental cerebral ischemia. *Magn. Reson. Imaging* 11, 241–246.
- Hirbec, H., Teilhac, J., Kamenka, J., Privat, A., Vignon, J., 2000. Binding properties of [3H]gacyclidine (cis(pip/me)-1-[1-(2-thienyl)-2-methylcyclohexyl]piperidine) enantiomers in the rat central nervous system. *Brain Res.* 859, 177–192.
- Holtz, A., Nystrom, B., Gerdin, B., Olsson, Y., 1990. Neuropathological changes and neurological function after spinal cord compression in the rat. *J. Neurotrauma* 7, 155–167.
- Inglis, B.A., Yang, L., Wirth III, E.D., Plant, D., Mareci, T.H., 1997. Diffusion anisotropy in excised normal rat spinal cord measured by NMR microscopy. *Magn. Reson. Imaging* 15, 441–450.
- Inglis, B.A., Neubauer, D., Yang, L., Plant, D., Mareci, T.H., Muir, D., 1999. Diffusion tensor MR imaging and comparative histology of glioma engrafted in the rat spinal cord. *Am. J. Neuroradiol.* 20, 713–716.
- Inglis, B.A., Bossart, E.L., Buckley, D.L., Mareci, T.H., 2001. Visualization of neural tissue water compartments using biexponential diffusion tensor MRI. *Magn. Reson. Med.* 45, 580–587.
- Jolesz, F.A., Polak, J.F., Adams, D.F., Ruenzel, P.W., 1987. Myelinated and nonmyelinated nerves: comparison of proton MR properties. *Radiology* 164, 89–91.
- Kim, J., Budde, M., Neil, J., Song, S.K., 2005. Reproducibility of in vivo DTI mouse spinal cord. *ISMRM*, 1978.
- Loubinoux, I., Volk, A., Borredon, J., Guirimand, S., Tiffon, B., Seylaz, J., Meric, P., 1997. Spreading of vasogenic edema and cytotoxic edema assessed by quantitative diffusion and T2 magnetic resonance imaging. *Stroke* 28, 419–426 (discussion 426–7).
- MacKay, A., Whittall, K., Adler, J., Li, D., Paty, D., Graeb, D., 1994. In vivo visualization of myelin water in brain by magnetic resonance. *Magn. Reson. Med.* 31, 673–677.
- Madi, S., Hasan, K.M., Narayana, P.A., 2004. Diffusion tensor imaging of in vivo and excised rat spinal cord at 7 T with an icosahedral encoding scheme. *Magn. Reson. Med.* 53, 118–125.

- Matsuzawa, H., Kwee, I.L., Nakada, T., 1995. Magnetic resonance axonography of the rat spinal cord: postmortem effects. *J. Neurosurg.* 83, 1023–1028.
- Moseley, M.E., Cohen, Y., Kucharczyk, J., et al., 1990. Diffusion-weighted MR imaging of anisotropic water diffusion in cat central nervous system. *Radiology* 176, 439–445.
- Moseley, M.E., Mintorovitch, J., Cohen, Y., et al., 1990. Early detection of ischemic injury: comparison of spectroscopy, diffusion-, T2-, and magnetic susceptibility-weighted MRI in cats. *Acta Neurochir., Suppl. (Wien)* 51, 207–209.
- Nevo, U., Hauben, E., Yoles, E., Agranov, E., Akselrod, S., Schwartz, M., Neeman, M., 2001. Diffusion anisotropy MRI for quantitative assessment of recovery in injured rat spinal cord. *Magn. Reson. Med.* 45, 1–9.
- Nossin-Manor, R., Duvdevani, R., Cohen, Y., 2002. q-Space high *b* value diffusion MRI of hemi-crush in rat spinal cord: evidence for spontaneous regeneration. *Magn. Reson. Imaging* 20, 231–241.
- Olby, N.J., Blakemore, W.F., 1996. Reconstruction of the glial environment of a photochemically induced lesion in the rat spinal cord by transplantation of mixed glial cells. *J. Neurocytol.* 25, 481–498.
- Peled, S., Cory, D.G., Raymond, S.A., Kirschner, D.A., Jolesz, F.A., 1999. Water diffusion, T(2), and compartmentation in frog sciatic nerve. *Magn. Reson. Med.* 42, 911–918.
- Petralia, R.S., Wang, Y.X., Wenthold, R.J., 1994. The NMDA receptor subunits NR2A and NR2B show histological and ultrastructural localization patterns similar to those of NR1. *J. Neurosci.* 14, 6102–6120.
- Pirko, I., Fricke, S.T., Johnson, A.J., Rodriguez, M., Macura, S.I., 2005. Magnetic resonance imaging, microscopy, and spectroscopy of the central nervous system in experimental animals. *NeuroRx* 2, 250–264.
- Prado, R., Dietrich, W.D., Watson, B.D., Ginsberg, M.D., Green, B.A., 1987. Photochemically induced graded spinal cord infarction. Behavioral, electrophysiological, and morphological correlates. *J. Neurosurg.* 67, 745–753.
- Siesjo, B.K., Wieloch, T., 1985. Cerebral metabolism in ischaemia: neurochemical basis for therapy. *Br. J. Anaesth.* 57, 47–62.
- Silver, X., Ni, W.X., Mercer, E.V., Beck, B.L., Bossart, E.L., Inglis, B., Mareci, T.H., 2001. In vivo 1H magnetic resonance imaging and spectroscopy of the rat spinal cord using an inductively-coupled chronically implanted RF coil. *Magn. Reson. Med.* 46, 1216–1222.
- Song, S.K., Yoshino, J., Le, T.Q., Lin, S.J., Sun, S.W., Cross, A.H., Armstrong, R.C., 2005. Demyelination increases radial diffusivity in corpus callosum of mouse brain. *NeuroImage* 26, 132–140.
- Sorensen, A.G., Wu, O., Copen, W.A., Davis, T.L., Gonzalez, R.G., Koroshetz, W.J., Reese, T.G., Rosen, B.R., Wedeen, V.J., Weisskoff, R.M., 1999. Human acute cerebral ischemia: detection of changes in water diffusion anisotropy by using MR imaging. *Radiology* 212, 785–792.
- Sotak, C.H., 2002. The role of diffusion tensor imaging in the evaluation of ischemic brain injury—a review. *NMR Biomed.* 15, 561–569.
- Steward, O., Schauwecker, P.E., Guth, L., Zhang, Z., Fujiki, M., Inman, D., Wrathall, J., Kempermann, G., Gage, F.H., Saatman, K.E., Raghupathi, R., McIntosh, T., 1999. Genetic approaches to neurotrauma research: opportunities and potential pitfalls of murine models. *Exp. Neurol.* 157, 19–42.
- Tator, C.H., Fehlings, M.G., 1991. Review of the secondary injury theory of acute spinal cord trauma with emphasis on vascular mechanisms. *J. Neurosurg.* 75, 15–26.
- Thornton, J.S., Ordidge, R.J., Penrice, J., Cady, E.B., Amess, P.N., Punwani, S., Clemence, M., Wyatt, J.S., 1997. Anisotropic water diffusion in white and gray matter of the neonatal piglet brain before and after transient hypoxia–ischaemia. *Magn. Reson. Imaging* 15, 433–440.
- Totoiu, M.O., Keirstead, H.S., 2005. Spinal cord injury is accompanied by chronic progressive demyelination. *J. Comp. Neurol.* 486, 373–383.
- Watson, B.D., Prado, R., Dietrich, W.D., Ginsberg, M.D., Green, B.A., 1986. Photochemically induced spinal cord injury in the rat. *Brain Res.* 367, 296–300.
- Webb, S., Munro, C.A., Midha, R., Stanis, G.J., 2003. Is multicomponent T2 a good measure of myelin content in peripheral nerve? *Magn. Reson. Med.* 49, 638–645.
- Whittall, K.P., MacKay, A.L., Graeb, D.A., Nugent, R.A., Li, D.K., Paty, D.W., 1997. In vivo measurement of T2 distributions and water contents in normal human brain. *Magn. Reson. Med.* 37, 34–43.